Received: 29 September 2016 | Accepted: 12 April 2017

DOI: 10.1002/hyp.11206

WILEY

RESEARCH ARTICLE

Interactions between groundwater and seasonally ice-covered lakes: Using water stable isotopes and radon-222 multilayer mass balance models

Marie Arnoux[1,2] | Elisabeth Gibert-Brunet[2] | Florent Barbecot[1] | Sophie Guillon[3] | John Gibson[4] | Aurélie Noret[2]

[1] GEOTOP, Université du Québec à Montréal, Montréal, Canada

[2] GEOPS, UMR 8148, CNRS-Université Paris Sud XI, Orsay, France

[3] MINES ParisTech, PSL Research University, Centre de Géosciences, Fontainebleau, France

[4] Alberta Innovates Technology Futures, Victoria, Canada

Correspondence
Marie Arnoux, GEOTOP, Université du Québec à Montréal, Montréal, Québec, H3C 3P8 Canada.
Email: marie.arnoux@u-psud.fr

Abstract

Interactions between lakes and groundwater are of increasing concern for freshwater environmental management but are often poorly characterized. Groundwater inflow to lakes, even at low rates, has proven to be a key in both lake nutrient balances and in determining lake vulnerability to pollution. Although difficult to measure using standard hydrometric methods, significant insight into groundwater–lake interactions has been acquired by studies applying geochemical tracers. However, the use of simple steady-state, well-mixed models, and the lack of characterization of lake spatiotemporal variability remain important sources of uncertainty, preventing the characterization of the entire lake hydrological cycle, particularly during ice-covered periods. In this study, a small groundwater-connected lake was monitored to determine the annual dynamics of the natural tracers, water stable isotopes and radon-222, through the implementation of a comprehensive sampling strategy. A multilayer mass balance model was found outperform a well-mixed, one-layer model in terms of quantifying groundwater fluxes and their temporal evolution, as well as characterizing vertical differences.

Water stable isotopes and radon-222 were found to provide complementary information on the lake water budget. Radon-222 has a short response time, and highlights rapid and transient increases in groundwater inflow, but requires a thorough characterization of groundwater radon-222 activity. Water stable isotopes follow the hydrological cycle of the lake closely and highlight periods when the lake budget is dominated by evaporation versus groundwater inflow, but continuous monitoring of local meteorological parameters is required. Careful compilation of tracer evolution throughout the water column and over the entire year is also very informative. The developed models, which are suitable for detailed, site-specific studies, allow the quantification of groundwater inflow and internal dynamics during both ice-free and ice-covered periods, providing an improved tool for understanding the annual water cycle of lakes.

KEYWORDS

geochemical tracers, groundwater-surface water interactions, lakes, multilayer mass balances, Québec (Canada), radon-222, water stable isotopes

1 | INTRODUCTION

An overall decrease in lake water quality has been observed in Quebec and in North America more generally, which recent assessments have attributed to changes in both the quantity and quality of groundwater inputs (Lewandowski, Meinikmann, Nützmann, & Rosenberry, 2015; Schilling, Streeter, Quade, & Skopec, 2016). Groundwater–lake interactions influence lake ecosystems, as well as the sensitivity and response of lakes to environmental changes, and the evolution of the quantity and/or quality of lake water (Arnoux et al., 2017; Kidmose et al., 2013; Shaw, White, & Gammons, 2013; Zhu & Schwartz, 2011). No direct indicator exists with which to estimate the connection of a lake to the related groundwater system and evaluating groundwater input to a lake can therefore be rather difficult.

Groundwater–lake interactions are not well understood and are commonly neglected in lake water budgets. This knowledge gap limits the understanding of regional hydrology, particularly in Québec, where lakes cover more than 10% of the land surface (MDDELCC, 2016).

An accurate water budget is necessary to identify real time changes in water quality and quantity and their causes, as well as to forecast the evolution of a lake and the connected groundwater system, and is therefore essential for freshwater resource management. The quantification of the different water budget terms of a groundwater-fed lake is difficult, and several approaches have been developed. These include hydrological models (Ala-aho, Rossi, Isokangas, & Kløve, 2015; Hunt, Haitjema, Krohelski, & Feinstein, 2003; Smerdon, Allen, Grasby, & Berg, 2009), artificial tracers, such as SF_6 (von Rohden et al., 2009), and naturally occurring tracers, such as water stable isotopes (Arnoux et al., 2017; Krabbenhoft, Bowser, Anderson, & Valley, 1990; Sacks, Lee, & Swancar, 2014; Stets, Winter, Rosenberry, & Striegl, 2010) and the radioactive gas, radon-222 (^{222}Rn; Corbett, Burnett, Cable, & Clark, 1997; Kluge, Ilmberger, von Rohden, & Aeschbach-Hertig, 2007; Schmidt et al., 2010). This paper focuses on water stable isotopes and ^{222}Rn, the most widely applied geochemical tracers.

The use of ^{222}Rn for tracing groundwater inflow into surface water is well known for investigating submarine groundwater discharge (Cable, Burnett, Chanton, & Weatherly, 1996; Baudron et al., 2015). However, the use of ^{222}Rn in lakes has only gained attention in recent years, probably due to generally low ^{222}Rn activity in lakes (in the range of a few Bq/m^3), in contrast to the high activity in groundwater (typically between 1,000 and 100,000 Bq/m^3). The first lake water budget based on ^{222}Rn was demonstrated by Corbett et al. (1997) and led to many subsequent applications (Cook et al., 2008; Gilfedder, Frei, Hofmann, & Cartwright, 2015; Gleeson, Novakowski, Cook, & Kyser, 2009; Kluge et al., 2007; Kluge et al., 2012; Malgrange & Gleeson, 2014). For simplicity, most studies assumed constant ^{222}Rn activity for the whole water column and disregarded vertical gradients related to lake stratification, although these are widely known to potentially be informative (Cook et al., 2008; Schmidt & Schubert, 2007). Stable isotopes of water have been used since the 1960s to determine lake water budgets (Dinçer & Davis, 1984; Gibson, 2002; Krabbenhoft et al., 1990; Turner, Allison, & Holmes, 1984). In recent years, several studies have used this tracer to quantify groundwater inflow to lakes but again assume a well-mixed water column (Arnoux et al., 2017; Isokangas, Rozanski, Rossi, Ronkanen, & Kløve, 2015; Sacks et al., 2014). A recent review of these approaches, particularly applications in regional studies, has been provided by Gibson, Birks, and Yi (2015).

Vertical gradients in ^{222}Rn and water stable isotope contents can be significant in lakes and can reveal important information, especially for locating sites of groundwater inflow. More complex approaches have already been published in the case of obvious stratification, where the lake was vertically subdivided into layers to mimic the stratification pattern (Kluge et al., 2012; Schmidt & Schubert, 2007).

The main objectives of the current work are (a) to determine the ^{222}Rn and ^{18}O/^{2}H dynamics in a small groundwater-connected lake and (b) to compare a depth-resolved, multilayer model and a well-mixed, one-layer model for ^{222}Rn and water stable isotope mass balances. The input of depth profiles measured under different stratification conditions for the quantification of groundwater inflow to the lake is discussed. This study also demonstrates that changes in groundwater fluxes over time can be tracked, and a better understanding of lake dynamics can thereby be established.

2 | STUDY SITE

Lake Lacasse is a small (27,164 m^2), dimictic glacial lake located in the Laurentians region of Quebec (Canada; Figure 1). It is a flow-through lake without any permanent inflow stream and with a single outlet stream flowing to the south (Figure 1). It has a maximum depth of 5.5 m, an average depth of 2.1 m, and a catchment area of 0.148 km^2. The lake lies on glacial deposits and crystalline

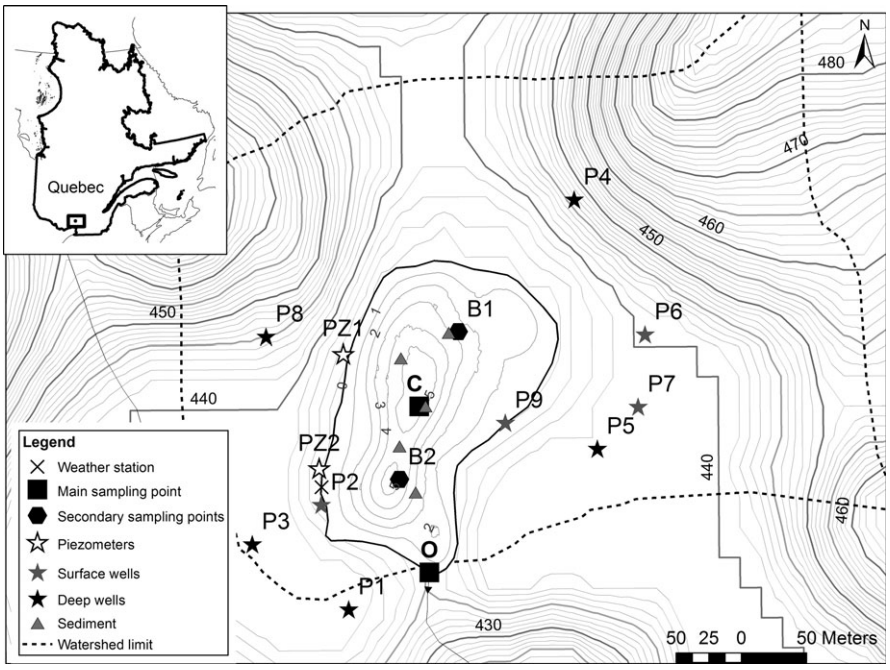

FIGURE 1 Location of water (lake and groundwater) and sediment sampling points, and bathymetry of Lake Lacasse. Insert: Location of Lake Lacasse, 15 km north of Saint-Faustin-Lac-Carré, in the Laurentides region of Québec, Canada

bedrock, including granitic igneous intrusive rocks, such as mangerite, farsundite, and monzonite of the Greenville province (SIGEOM). Glacial deposits consist of sandy till and fluvioglacial deposits that contain rock boulders.

3 | METHODS

3.1 | Field measurements

3.1.1 | Instrumentation

Meteorological data, including atmospheric humidity and temperature, precipitation, solar radiation, wind speed, and wind direction were recorded every 15 min for a period of 1 year, from August 2015 to June 2016, at a weather station platform (Davis) located on the south-western lake shore (Figure 1). Meteorological data from the Saint-Faustin-Lac-Carré meteorological station, located 15 km south of the lake, were used when no meteorological data were recorded at the lake shore station. Water levels from wells, the lake, and the outlet stream were continuously recorded by level loggers (Figures 1 and 3). The volume of the lake was estimated from a bathymetric map obtained by kriging shoreline positions and depth profiles measured with a Speedtech Depthmate Portable Sounder (Figure 1).

3.1.2 | Water sampling

Electrical conductivity and pH of lake water were measured with a depth interval of 0.5 m using a peristaltic pump, flow-through cell, and single-parameter sensors (WTW). Electrical conductivity was measured according to the Hanna instrument standard HI 70031, and pH according to the Hanna instrument standards HI 70004, 70007, and 70010. Water temperature was measured in situ within the water column using a Hanna multi-parameter probe, also at 0.5-m depth intervals (Figure 4).

Water samples were collected from the lake at 2-week to 1-month intervals. Water stable isotopic compositions (δ^2H and $\delta^{18}O$; Figure 2) and ^{222}Rn activity of all samples were measured. Lake water samples were collected from point C (Figure 1), corresponding to the deepest part of the lake, during all sampling campaigns, and supplemented by samples at points B1 and B2 during some campaigns. Sampling was performed at fixed depths (0.5, 2.5, 3.5, and 4.5 m) in order to monitor the vertical heterogeneity of the water column, using a peristaltic pump. Isotopic compositions of lake water samples (δ^2H and $\delta^{18}O$) were linearly correlated, and the Local Evaporation Line was determined through regression of lake isotopic values (Figure 2). Water from the outlet stream was also sampled as part of each sampling campaign at point O (Figure 1). These samples were collected from the middle of the channel, and flow rate was measured using the dilution gauging method, with constant injection of a saline solution (Figure 3). Groundwater was sampled twice from private wells in the vicinity of the lake (Figure 1). Untreated tap water was collected after purging the system. Unfiltered water samples were stored in 35- and 250-ml bottles for stable isotope and ^{222}Rn analyses, respectively.

Samples to determine the rain water isotopic composition (Figure 2) were collected in a rain collector designed to prevent water evaporation, as described by Gröning et al. (2012). One cumulative rain sample and corresponding volume-weighted isotopic composition of precipitation was obtained per field campaign. These data were used to obtain the Local Meteoric Water Line, determined through regression of rain water isotopic samples (Figure 2).

Water stable isotopic compositions were measured with a Laser Water Isotope Analyser (OA ICOS DLT, Los Gatos Research, now ABB) at the University of Paris-Sud/Paris-Saclay (Orsay, France). The accuracy of measurements is ±1‰ for δ^2H and ±0.2‰ for $\delta^{18}O$. Results are reported in δ values, representing deviations in per mil (‰) from the isotopic composition of the international standard (Vienna Standard Mean Ocean Water, VSMOW), such that δ^2H or $\delta^{18}O = ([R_{sample}/R_{VSMOW}] - 1) \times 1{,}000$, where R refers to $^2H/H$ or $^{18}O/^{16}O$ ratios. The ^{222}Rn activity in water was measured at University of Quèbec in Montreal (UQAM; Montreal, Canada) within 3 days of sampling, using liquid scintillation counting with extraction, according to the method described by Lefebvre, Barbecot, Ghaleb, Larocque, and Gagne (2013).

3.1.3 | Ice and snow sampling

The isotopic composition of lake ice was obtained from ice cores collected in December 2015 (Figure 2). The mean ice isotopic composition is −54.37‰ for δ^2H and −7.4‰ for $\delta^{18}O$. Ice thickness was 3 cm on December 17th, reached a maximum of 52 cm on March 23rd, and was 40 cm on April 18th when the melt period started. The mean isotopic composition of snow was determined for snow cores collected during each campaign, and was highly variable, as illustrated in Figure 2. In the model, the mean isotopic composition of two snow cores (40 and 45 cm) taken on the lake shore on April 18th was used; δ^2H = −103.7‰ and $\delta^{18}O$ = −54.37‰. The total volumes of water from melting ice and snow were estimated to be approximately 10,000 and 11,000 m^3, respectively.

3.1.4 | Sediment sampling and ^{222}Rn diffusive flux determination

The ^{222}Rn flux across the sediment–water interface is needed for the ^{222}Rn mass balance and is commonly determined through sediment equilibration experiments (Corbett, Burnett, Cable, & Clark, 1998; Kluge et al., 2012). To account for small-scale heterogeneities in the sediment and for representativeness, samples were taken with a sediment corer at five locations distributed across the lake (Figure 1). Following the protocol described in Corbett et al. (1998), an average of 66 g of dry sediment was transferred to 1-L glass bottles, subsequently filled with distilled water, and capped. The five bottles were then left for more than 1 month to allow the radium–radon equilibrium to be reached. The water overlying the sediment was then collected and its ^{222}Rn activity was measured using liquid scintillation counting with direct extraction, according to the method described by Lefebvre et al. (2013). Equilibration experiments and analyses were performed at a constant laboratory temperature of 20 °C. The diffusive flux from the sediment into the lake was then estimated by

$$F_{sed}A_{sed} = (\lambda_{Rn}D_{sed})^{1/2}(C_{eq} - \phi C_0) \quad (1)$$

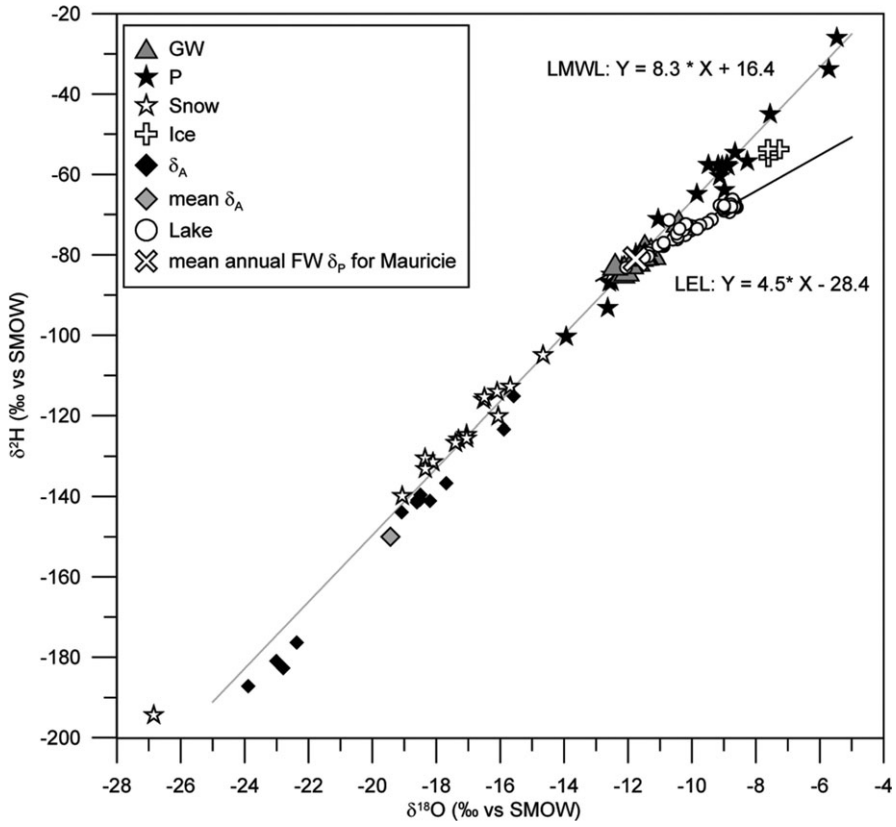

FIGURE 2 $\delta^{18}O$ and $\delta^{2}H$ values measured in lake water, groundwater, rain, snow, and ice from the lake surface. Isotopic composition of atmospheric water vapour calculated from meteorological data. Local Meteoric Water Line (LMWL) and Local Evaporation Line (LEL) determined by regression on rain and lake samples respectively. Samples were taken between June 2015 and May 2016

where F_{sed} is the flux of ^{222}Rn from the sediment ($Bq{\cdot}m^2{\cdot}s^{-1}$) through a given surface area, A_{sed} (m^2); λ_{Rn} is the ^{222}Rn radioactive decay constant (s^{-1}); D_{sed} is the bulk diffusion coefficient in the wet sediment (m^2/s); C_{eq} is the ^{222}Rn activity measured in the sediment equilibration experiments (Bq/m^3); C_0 is the ^{222}Rn activity in lake water at the sediment–water interface (Bq/m^3); and ϕ is the sediment porosity, here equal to 0.9. C_0 was assumed to be equal to the minimum ^{222}Rn activity measured in the lake (20 ± 10 Bq/m^3). The bulk diffusion coefficient was set as equal to $D_{sed} = 10^{-9}$ m^2/s, an average value consistent with previous studies (0.8×10^{-9} m^2/s [Imboden & Joller, 1984; Kluge et al., 2012], $1.0 \pm 0.3 \times 10^{-9}$ m^2/s [Corbett et al., 1998], from 4.9 to 7.2×10^{-10} m^2/s [Baudron et al., 2015]). A mean value of 0.7 ± 0.2 $Bq{\cdot}m^{-2}{\cdot}day^{-1}$ was obtained for the diffusive ^{222}Rn flux from the sediment.

3.2 | Water mass balance

The lake water budget allows fluxes between groundwater and surface water to be quantified and is described by

$$\frac{dV}{dt} = I - E - Q \tag{2}$$

where V is the volume of the lake (m^3); t is time (days); E is evaporation (m^3/day); I is the instantaneous inflow (m^3/day) and is the sum of upstream surface inflow (I_S; zero for the studied lake), runoff from the catchment area (I_R; considered negligible), groundwater inflow (I_G), and precipitation on the lake surface (P); Q is instantaneous outflow (m^3/day), which is the sum of surface (Q_S) and groundwater (Q_G) outflows. Under constant atmospheric and hydrologic conditions, steady state is assumed, such that $dV/dt = 0$, and thus $I_G = Q_S + Q_G + E - P$ for the entire lake.

3.3 | Stable isotopic mass balance

For water stable isotopes, the lake isotopic mass balance is

$$V\frac{d\delta_L}{dt} + \delta_L\frac{dV}{dt} = I\delta_I - E\delta_E - Q\delta_Q \tag{3}$$

where δ_L is the isotopic composition of the lake; δ_I, δ_S, δ_R, δ_G, and δ_P are the isotopic compositions of total inflow and its components (upstream surface inflow, runoff, groundwater inflow, and precipitation), respectively; and δ_Q, δ_{QS}, and δ_{QG} are the isotopic compositions of the total outflow and its components (surface and groundwater outflow), respectively. The isotopic compositions of lake, rain, and surface outflow water (δ_L, δ_P, and δ_{QS}) were measured in the field, as described above.

The isotopic composition of evaporating water (δ_E) was not measured but instead estimated using the Craig and Gordon (1965) model, given by Gonfiantini (1986) as

$$\delta_E = \frac{(\delta_L - \varepsilon^+)/\alpha^+ - h\delta_A - \varepsilon_K}{1 - h + 10^{-3}\varepsilon_K} \tag{4}$$

where h is the relative humidity at the lake surface (decimal fraction) measured at the weather station, δ_A is the local isotopic composition of the atmospheric moisture (‰); $\varepsilon^+ = (\alpha^+ - 1)^*1,000$ and is the equilibrium isotopic separation (‰), where α^+ is the equilibrium isotopic fractionation, $\varepsilon_K = C_K(1 - h)$ is the kinetic isotopic separation (‰), and C_K is the ratio of molecular diffusivities between heavy and light molecules (Gibson et al., 2015). In this study, C_K values representative of fully

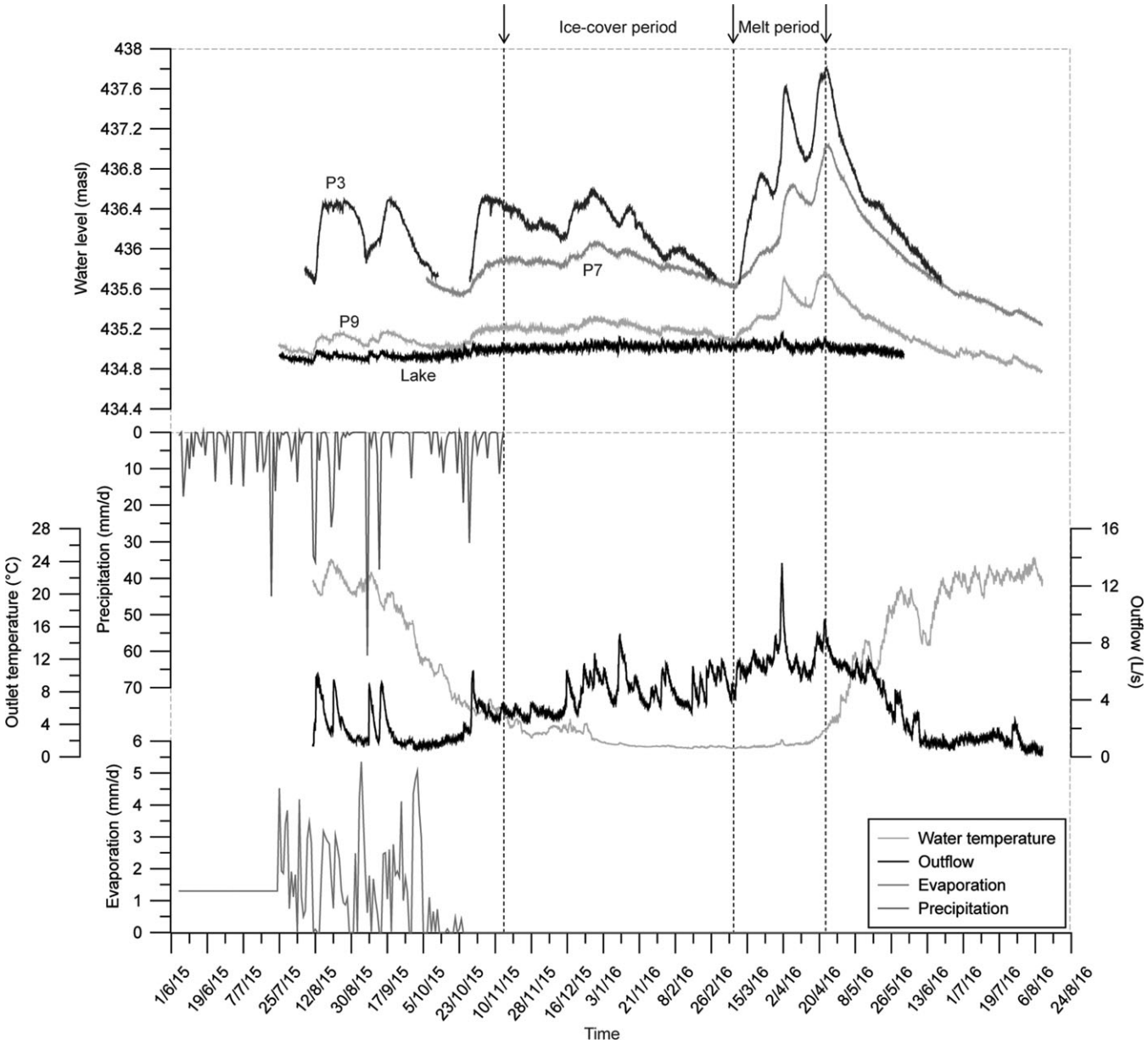

FIGURE 3 Water level of wells P3, P7, P9, and of the lake; flow rate and temperature of the lake outlet; precipitation and evaporation used in the isotopic model

turbulent wind conditions and a rough surface, as occurred on Lake Lacasse, were used: C_K = 14.2‰ for oxygen and C_K = 12.5‰ for hydrogen, based on experimental data (Horita, Rozanski, & Cohen, 2008). Experimental $\delta^{18}O$ and $\delta^{2}H$ values of Horita and Wesolowski (1994) were used for equilibrium fractionation factors:

$$\alpha^{+}\left({}^{18}O\right) = \exp\left(-7.685/10^{3} + 6.7123/T - 1,666.4/T^{2} + 350,410/T^{3}\right) \quad (5)$$

$$\alpha^{+}\left({}^{2}H\right) = \exp\left(1158.8\times T^{3}/10^{12} - 1620.1\times T^{2}/10^{9} + 794.84\times T/10^{6} - 161.04/10^{3} + 2999200/T^{3}\right) \quad (6)$$

where T is temperature (K).

The isotopic composition of atmospheric moisture (δ_A, ‰) was calculated assuming equilibrium isotopic exchange between precipitation and vapour:

$$\overline{\delta_A} = \frac{\overline{\delta_P} - \overline{\varepsilon^{+}}}{1 + 10^{-3}\overline{\varepsilon^{+}}} \quad (7)$$

where $\overline{\delta_P}$ (‰) is the mean annual isotopic composition of precipitation, determined for collected rain samples. A mean annual value of $\delta_A{}^{2}H$ = −150‰ and $\delta_A{}^{18}O$ = −19.4‰ was calculated and used in the model.

Substitution of Equation 4 into Equation 3, assuming well-mixed conditions in the lake, yields

$$V\frac{d\delta_L}{dt} + \delta_L\frac{dV}{dt} = P\delta_P + I_G\delta_G - Q\delta_L - \frac{E}{1-h+10^{-3}\varepsilon_K}\left(\frac{\delta_L - \varepsilon^{+}}{\alpha^{+}} - h\delta_A - \varepsilon_K\right) \quad (8)$$

A steady state was assumed, such that dV/dt = 0. Equation 8 can therefore be simplified to

$$V\frac{d\delta_L}{dt} = P\delta_P + I_G\delta_G - (P + I_G - E)\delta_L - \frac{E}{1-h+10^{-3}\varepsilon_K}\left(\frac{\delta_L - \varepsilon^+}{\alpha^+} - h\delta_A - \varepsilon_K\right) \quad (9)$$

Thus, the isotopic composition of the lake at time $t + dt$ was expressed as a function of its value at the previous time step, t, and of parameters:

$$\delta_L{}^{t+dt} = \frac{A}{B} + \left(\delta_L{}^t - \frac{A}{B}\right)\exp\left(-\frac{B}{V}dt\right) \quad (10)$$

with

$$A = P\delta_P + I_G\delta_G - \frac{E}{1-h+10^{-3}\varepsilon_K}(-h\delta_A - \varepsilon_K - \varepsilon^+/\alpha^+) \quad (11)$$

$$B = P + I_G - E\left(1 - \frac{1}{\alpha^+\left(1-h+10^{-3}\varepsilon_K\right)}\right) \quad (12)$$

Evaporation was calculated daily as a function of meteorological data, such as radiation, atmospheric temperature and humidity, lake temperature, and wind speed, using the Penman formula (Alazard, Leduc, Travi, Boulet, & Ben, 2015). During June and July 2015, no meteorological data were recorded at the local station, and a fixed value of E = 35 m^3/day was chosen as being representative of this interval. The mean value of groundwater isotopic composition, δ_G, was determined based on water samples from the private wells around the lake and is $\delta_G{}^2H$ = −81‰ and $\delta_G{}^{18}O$ = −11.7‰. As expected, this value equals the mean annual amount-weighted isotopic composition of precipitation calculated from the Global Network of Isotopes in Precipitation and *Programme d'Acquisition de Connaissances sur les Eaux Souterraines* (Program for Groundwater Knowledge Acquisition) datasets in the region, and falls close to the intersection between the Local Meteoric Water Line and the Local Evaporation Line (Figure 2). This mean groundwater value was determined using wells that are potentially in the upstream but also in the downstream flow path of the lake. Although this could be a limitation, steps have been taken to ensure that they are not directly influenced by lake water. Therefore, it should be representative of regional groundwater and not at risk of a spurious model or data feedback.

All parameters can therefore be measured or calculated with the exception of groundwater inflow and outflow, and a daily model based on the above equations was developed to calculate the isotopic composition of the lake. Groundwater inflow was adjusted to obtain the best fit of calculated $\delta^{18}O$ with respect to the measured values (Figures 8 and 9). As the field campaigns were not daily, extrapolation between two sampling times was necessary: Constant groundwater inflow values between sampling times were assumed most of the time, except when sampling intervals were large. In this case, groundwater inflow fluctuation was assumed based on water level fluctuations measured with loggers in nearby wells (Figure 3). During the ice-covered period (from mid-November to mid-May), evaporation and precipitation were set to 0 in the lake model. During the melt period (from mid-April to mid-May), snow melt from the catchment area and ice melt from the lake surface (see Section 3.1.1) were added to the isotopic calculation of the mass balance model.

First, a well-mixed, one-layer model was established, and the volume-weighted isotopic compositions in the lake were fitted. Then, as vertical gradients can provide additional information, a more detailed multilayer model was used to determine groundwater fluxes with depth. The same equations were used to calculate the isotopic composition in each layer, but evaporation and precipitation were set to affect only the surface layer. The lake was divided into four layers, as described in Table 1. According to the stratification of the water column (Figure 4), surface layers were sometimes mixed together to account for the evaporation enrichment observed in the deeper layers. The lake was therefore divided into three layers at the beginning of summer (from June to mid-August), two layers at the end of summer (from mid-August to the end of September), one layer during autumn mixing (from the end of September to mid-November), and, finally, four layers during the ice-covered period (from mid-November to May). When layers were mixed together, the mean volume-weighted isotopic composition was fitted, and the sum of all mixed layer volumes was considered in the calculation.

3.4 | ^{222}Rn mass balance

The ^{222}Rn mass balance can be calculated as per the following equation (Corbett et al., 1997; Kluge et al., 2012):

$$C_L\frac{dV}{dt} + V\frac{dC_L}{dt} = I_GC_G + F_{sed}A_{sed} - F_{surf}A_L - \lambda_{Rn}VC_L - QC_L \quad (13)$$

where C_L is the ^{222}Rn activity of the lake water (Bq/m^3); C_G is the average activity of the inflowing groundwater (Bq/m^3); F_{sed} is the ^{222}Rn flux (Bq·m^{-2}·day^{-1}) due to Rn diffusion from the sediment through a surface area, A_{sed} (in m^2); F_{surf} is the degassing flux at the lake surface (Bq·m^{-2}·day^{-1}); A_L is the area of the lake (m^2); and λ_{Rn} is the ^{222}Rn radioactive decay constant (day^{-1}). The ^{222}Rn activity is assumed to be zero in both the atmosphere and in precipitation. Radium is bound to sediment particles in fresh water (Kiro, Yechieli, Voss, Starinsky, & Weinstein, 2012), and radium activity in lake water is very low, such that ^{222}Rn production from radium decay is considered negligible.

The activity in the lake was first calculated using a well-mixed, one-layer model, and groundwater fluxes were determined to fit the volume-weighted ^{222}Rn activity, as for the isotopic model. A mean

TABLE 1 Characteristics of the four layers used in the models

Layer depth (from–to; m)	Layer volume (m^3)	Interface area between layers (m^2)	Interface area with sediments (m^2)	Layer height (m)
0–2	42,380	27,164	15,968	2
2–3	11,195	11,195	3,863	1
3–4	7,333	7,333	3,001	1
4–5.5	6,498	4,332	4,332	1.5

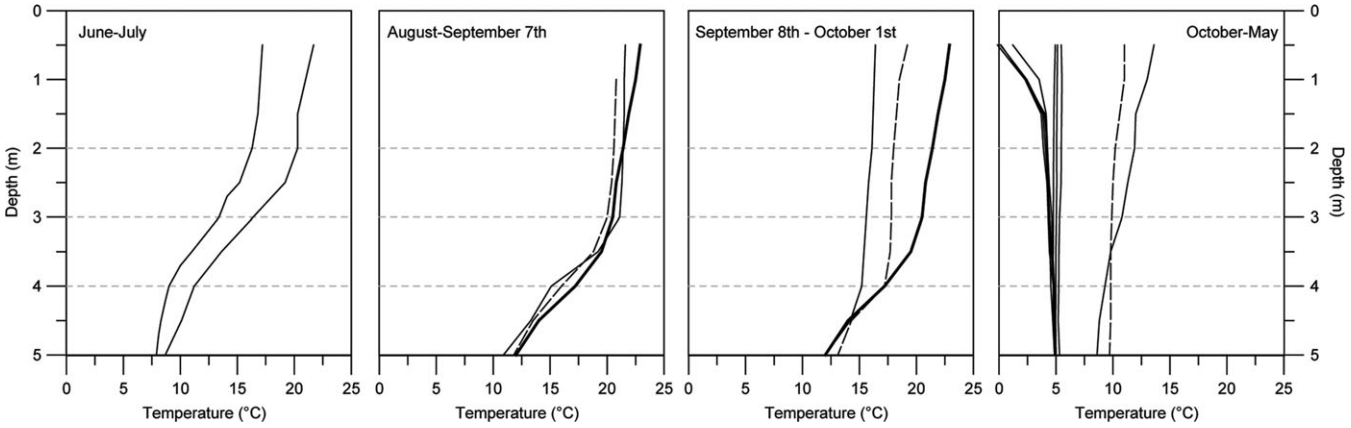

FIGURE 4 Evolution of temperature versus depth in Lake Lacasse during the year 2015–2016

value equal to 12,572 Bq/m^3 was used for groundwater activity, obtained from measurements in the wells around the lake (Figure 1). As the activity in groundwater was observed to be highly variable in space, a sensitivity analysis was conducted (Section 4.3.3). This variability, not dependant on well depth, is probably due to the local geology. Degassing to the atmosphere was considered to be negligible during the ice-covered period (from mid-November to mid-May).

The lake was then divided in four layers (Table 1) for the entire year, except during autumn mixing (end of September), when the lake activity in all layers was set to be equal to the mean volume-weighted isotopic composition of the lake. A diffusive vertical exchange between adjacent layers was calculated according to Fick's first law and was added to the mass balance. Assuming a steady state ($dV/dt = 0$), Equation 13 was modified to satisfy this extension of the model. Evolution of ^{222}Rn activity in layer i is expressed as

$$V_i\frac{dC_i}{dt} = I_{G,i}C_G + F_{sed}A_{sed,i} - \lambda_{Rn}V_iC_i - Q_iC_i + A_{i-1}K_{i-1}\frac{dC}{dz}\Big)_{i-1\to i} - A_iK_i\frac{dC}{dz}\Big)_{i\to i+1} \quad (14)$$

where C_i is the ^{222}Rn activity in the lake water in layer i (Bq/m^3); V_i is the layer volume (m^3); $I_{G,i}$ is the groundwater inflow into layer i (m^3/day); $A_{sed,i}$ is the contact area between sediment and water in layer i (m^2). C_G is assumed to be constant across all depths. $K_{i-1}\frac{dC}{dz})_{i-1\to i}$ is the diffusion flux (Bq·m^{-2}·day^{-1}), with K_{i-1} the diffusion coefficient (m^2/day), between layer $i-1$ and i through the interface A_{i-1} (m^2). Therefore, for the multilayer ^{222}Rn mass balance model, the following equation was solved for each layer and time step:

$$C_i^{t+dt} = \left(I_{G,i}^{t+dt}C_G + F_{sed}A_{sed,i} - \lambda_{Rn}V_iC_i^t - I_{G,i}C_i^t + A_{i-1}K_{i-1}\right. \quad (15)$$
$$\left.\left(C_{i-1}^t - C_i^t\right) - A_iK_i\left(C_i^t - C_{i+1}^t\right)\right)/V_i + C_i^t$$

where C_i^{t+dt} is the ^{222}Rn activity in the layer i at time $t + dt$ and C_i^t at time t (Bq/m^3).

The ^{222}Rn diffusion coefficient in water (K_i) depends on the stratification of the water column. For weak stratification conditions, K was set to 10^{-6} m^2/s (Kluge et al., 2012). During periods of stratification, the diffusion between layers located on either side of the thermocline was calculated using a coefficient, K, equal to 10^{-9} m^2/s. The ^{222}Rn activity gradient depends on the difference in activity between the two layers considered. At the interface between the lake surface (A_s) and the atmosphere, the diffusive flux becomes kC_sA_s, with C_s the ^{222}Rn activities in surface water (Bq/m^3) and k the gas exchange velocity (m/day). The empirical relationship between k and wind speed proposed by MacIntyre, Wanninkhof, and Chanton (1995) and Turner, Malin, Nightingale, and Liss (1996) was used:

$$\text{For } u_{10} \leq 3.6\ m/s, k = 0.45u_{10}^{1.6}(Sc/600)^{-2/3} \quad (16)$$

$$\text{For } u_{10} > 3.6\ m/s, k = 0.45u_{10}^{1.6}(Sc/600)^{-0.5} \quad (17)$$

where k is expressed in cm/hr; u_{10} is the wind speed at 10-m height (m/s), and Sc is the Schmidt number for ^{222}Rn (i.e., the ratio of the kinematic viscosity of water to the molecular diffusion coefficient of ^{222}Rn, calculated for the conditions of salinity and temperature of Lake Lacasse, according to Wanninkhof [1992]). The wind speed at 10 m was calculated from the wind speed at 2 m using a simple wind power law with a wind shear coefficient for lakes, typically equal to 0.1. At wind speeds of only a few m/s or less, the determination of k and the gas exchange at the lake surface is quite difficult and the associated uncertainty is higher (Kluge et al., 2012).

4 | RESULTS

4.1 | Representativeness of the lake sampling

As can be seen in Figure 5, the horizontal variability of the lake was first verified during the highly stratified period (June 26, 2015) on a horizontal grid of 20 to 40 m and on profiles with depth intervals of 0.5 m (Figure 4). Temperature, pH, and electrical conductivity are used as proxies for the horizontal homogeneity of the lake. For most sampling points, the same trends with depth are observed and confirm the horizontal homogeneity of the lake. Indeed, an increase in electrical conductivity is observed with depth (from around 75 µS/cm at 0.5 m to around 105 µS/cm at 5 m), in addition to a decrease in temperature (from around 21 °C at 0.5 m to around 8 °C at 5 m) and in pH (from around 7.5 at 0.5 m to around 6.5 at 5 m). It can therefore be assumed that this small lake, with no surface inflow, is horizontally well mixed.

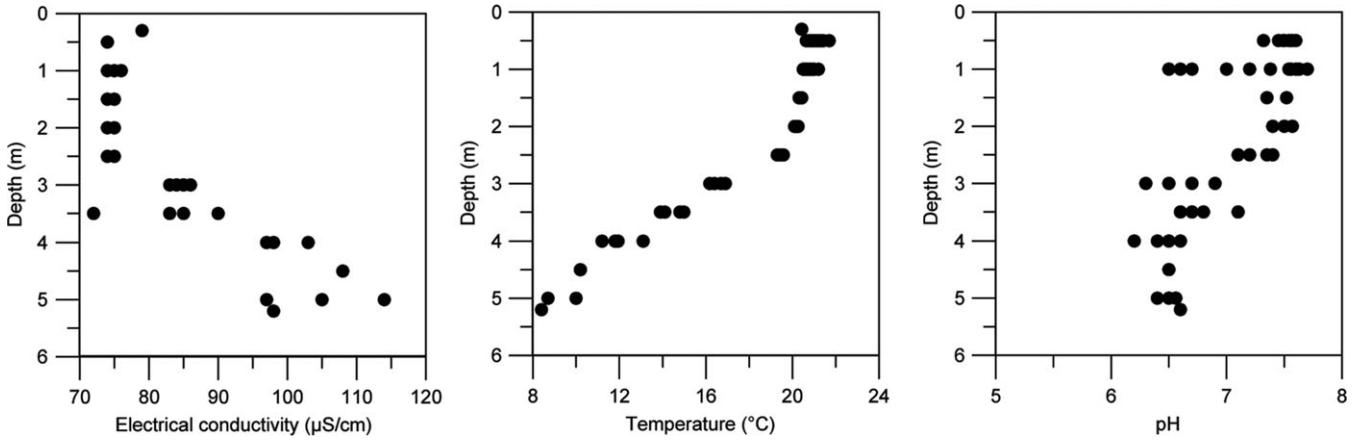

FIGURE 5 Electrical conductivity (EC), temperature (T), and pH measured at various depths in the lake during a period of high stratification (June 26, 2015). Depth profiles were measured throughout the lake on a 20 to 40–m grid (n = 68 for EC and T, and n = 61 for pH)

Water samples were collected at B1 and B2 (Figure 1), on either side of the lake centre (C), and also at the outlet stream (O), at various times, and from the lake centre during each sampling campaign. A strong correlation (r^2 > .94) in isotopic compositions is observed between the centre and the three other locations (B1, B2, and the outlet stream), across depths and sampling times (Figure 6). Horizontal homogeneity of water stable isotopes thus persists in the lake throughout the year, consistent with the smooth temporal variability of water stable isotopes driven by groundwater input. The ^{222}Rn activity has higher horizontal variability (r^2 = .75 between sites for given times and depths), especially in the low-activity range (^{222}Rn activity below 200 Bq/m^3), but the assumption of a horizontally well-mixed lake is justified for both tracers.

4.2 | Groundwater connection highlighted by water stable isotopes and radon-222

Evolution of δ^{18}O at various depths in the lake is shown in Figure 7. The δ^2H evolution was found to be very similar (Figure 9). therefore, water stable isotopes (^{18}O and ^{2}H) are considered as one tracer and are used in the same way. Lake monitoring began in early June, corresponding to the end of spring mixing. In the recently mixed lake, the isotopic composition was vertically homogeneous (δ^{18}O = −10.5‰), with a slight enrichment already notable, due to evaporation at the lake surface. A few weeks later, the isotopic composition of the surface water became more enriched, due to evaporation (δ^{18}O = −9.5‰), while the deepest water became isotopically depleted and closer to the mean isotopic composition of groundwater (δ^{18}O = −11.5‰), demonstrating groundwater inflow into the deep part of the lake. In August, the surface water became more enriched and the deep water mean isotopic composition reached that of groundwater. The maximum enrichment was reached at the surface at the beginning of August (δ^{18}O = −9.3‰). Surface enrichment then stopped, although there was still evaporation, due to an apparent equilibrium between evaporation and groundwater inflow. At the end of September, the isotopic composition of the deepest part of the lake began to enrich, resulting from the initiation of the autumn mixing. By mid-October, the lake was completely mixed, and the final isotopic composition was equal to the volume-weighted mean isotopic composition of the lake (δ^{18}O = −9.3‰), validating a depth–area relationship corresponding to the observed V-shape of the lake (Figure 1). Indeed, the isotopic composition of the deep water had a negligible influence on the mean value compared with the

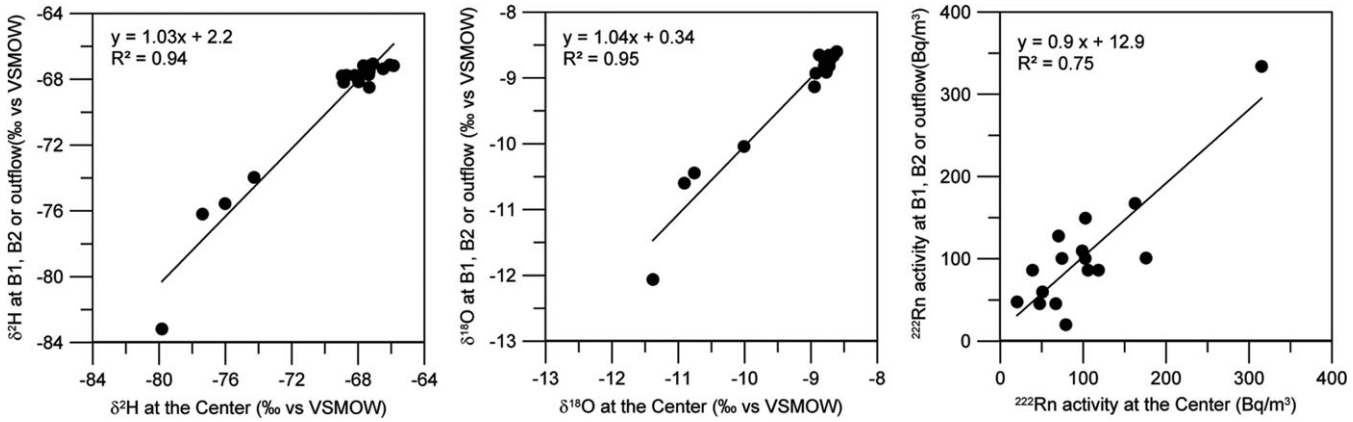

FIGURE 6 Comparisons of δ^2H, δ^{18}O, and ^{222}Rn activity measured at B1, B2, and C in the lake, and at the outlet stream, at the same depth and time. The outlet is compared to samples at C at 0.5 m; B1 and B2 are compared to samples at C at equivalent depths (n = 21 for stable isotopes and n = 16 for ^{222}Rn)

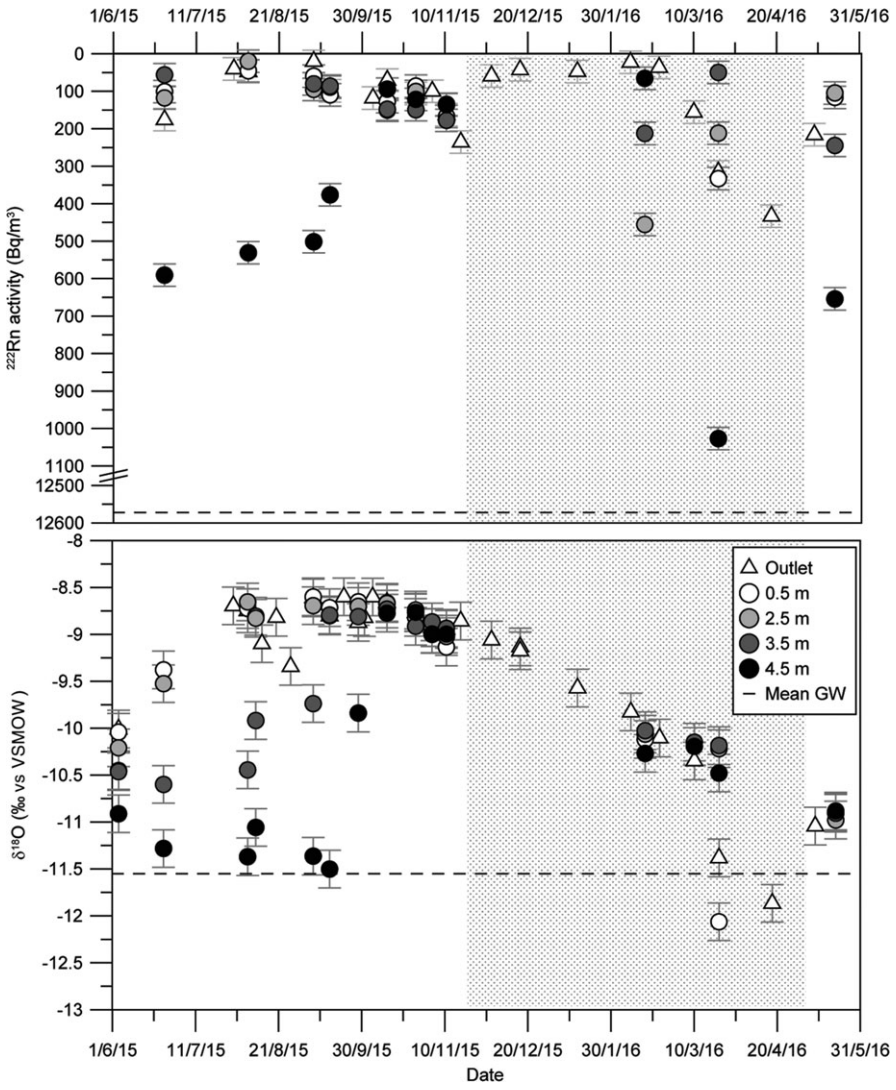

FIGURE 7 Evolution of $\delta^{18}O$ and ^{222}Rn activity measured at various depths at point C in Lake Lacasse. The ice-covered period, from November 15th to May 10th, is represented by the grey area

composition of surface layer. Until the formation of ice cover, the isotopic composition remained constant and was only slightly influenced by precipitation. During the ice-covered period, the isotopic composition slowly decreased in response to groundwater inflow and finally returned to the value measured following the previous spring mixing (i.e., in June 2015; $\delta^{18}O = -11‰$). During the ice-covered period, surface isotopic compositions were occasionally surprisingly depleted (e.g., on March 23rd). This was due to the rapid formation of ice at the lake surface, with a highly enriched isotopic composition (see Figure 2). The isotopic composition at the outlet (Figure 7) showed variations similar to those at the lake surface.

Evolution of ^{222}Rn activity at various depths is shown in Figure 7. During summer and autumn, ^{222}Rn activity followed the same dynamics as the stable isotopic composition, with higher activity in the deep water (approximately 600 Bq/m^3) than in the rest of the water column (close to 100 Bq/m^3), indicating groundwater inflow. By the end of September, ^{222}Rn activity of the deep water decreased, reaching that at the surface by mid-October (approximately 100 Bq/m^3), corresponding to autumn mixing. When the ice formed, ^{222}Rn activity increased slightly over the entire water column, reaching 150 to 250 Bq/m^3. In the outlet stream, ^{222}Rn activity remained low during the ice-covered period, until the end of February, and then increased until the melt period (to a measured maximum of 318 Bq/m^3), and finally decreased to its original value by the beginning of May (approximately 200 Bq/m^3). The lake surface (depth of 0.5 m) seemed to follow similar variations. However, the three other depths sampled (2.5, 3.5, and 4.5 m) showed different trends under ice cover. An inversion of the ^{222}Rn activity vertical gradient was observed on February 16th, with the highest value (456 Bq/m^3) at 2.5-m depth, an intermediate value (213 Bq/m^3) at 3.5 m, and the lowest activity (66 Bq/m^3) at 4.5-m depth. This inversion persisted until March 23rd, except at 4.5-m depth, where an impressively high value of 1,026 Bq/m^3 was measured. The overall increase in ^{222}Rn activity during the ice-covered period was related to groundwater inflow and the suppression of exchange with the atmosphere. After the melt period, ^{222}Rn activities at all depths returned to their values of the previous spring.

4.3 | Groundwater inflow dynamics

4.3.1 | Water stable isotope-based model

As described in Section 3.3, a model of lake isotopic composition (δ_L) with a daily time step was proposed, and groundwater inflow (I_G) was determined so as to achieve the closest match between the measured and modelled values of δ_L. A mean groundwater

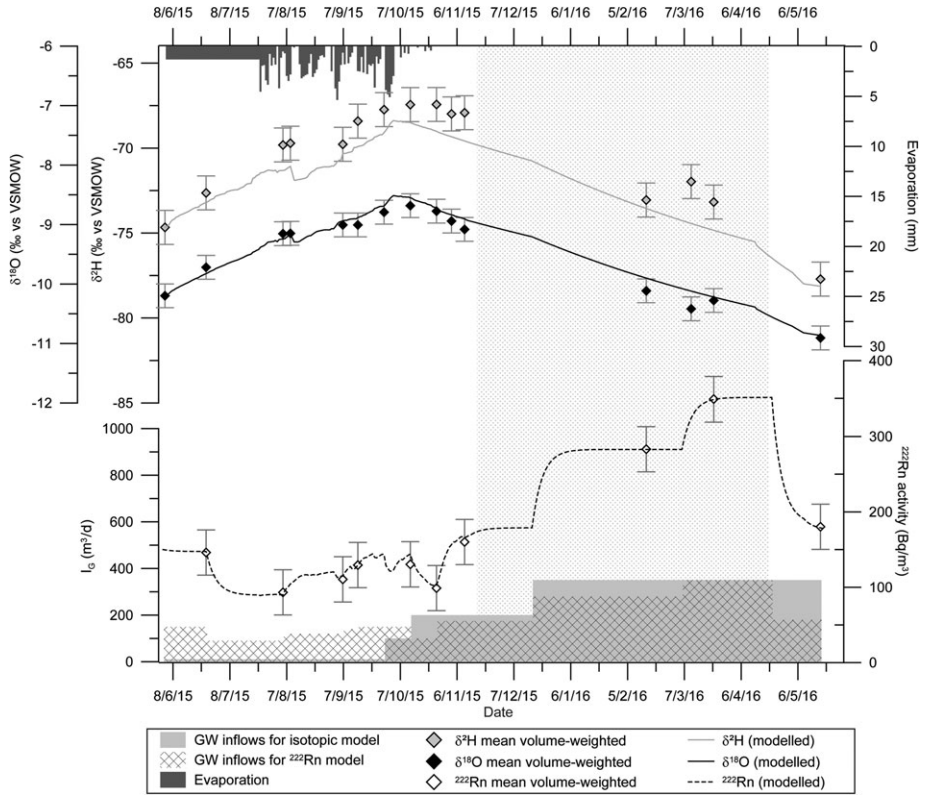

FIGURE 8 Results of the well-mixed one-layer isotopic and radon models fitted to mean volume weighted data; the ice-covered period, from November 15th to May 10th, is represented by the grey area

inflow of 198 m^3/day was obtained with the well-mixed, one-layer model (Figure 8).

The results of the isotopic mass balance multilayer model are shown in Figure 9. From June to mid-August, a mean I_G of 4 m^3/day was found for the 0- to 3-m layer and of 10 m^3/day for the 3- to 4-m layer. A mean I_G of 135 m^3/day was then fit from mid-August to the end of September for the 0- to 4-m layer. For the 4- to 5.5-m layer, a mean I_G of 100 m^3/day was determined to explain the data from June to the end of September. During autumn mixing (from the end of September to mid-November), a mean groundwater inflow of 281 m^3/day was needed to account for the data at the entire lake scale. During the ice-covered period, from mid-November to mid-April, I_G was equal to 228, 60, 40, and 35 m^3/day for the 0- to 2-m, 2- to 3-m, 3- to 4-m, and 4- to 5.5-m layers, respectively. I_G was consistent in the deep layers during the melt period (from mid-April to mid-May) and varied only in the surface layer. Mean I_G in the surface layer (i.e., the 0- to 2-m layer) was found to be 200 m^3/day from mid-November to mid-March, then 300 m^3/day from mid-March to mid-April, and, finally, 147 m^3/day from mid-April to mid-May.

For the entire modelled period, a mean groundwater inflow of 164 m^3/day was obtained for the surface layer (0- to 2-m layer), with lower input in summer than in winter, while a mean I_G of 57 m^3/day explains the evolution of the isotopic composition in the deepest layer (4- to 5.5-m layer), with higher input in summer than in winter (Figure 9). Finally, by summing the values of the different layers, a mean annual groundwater inflow of 276 m^3/day was required to fit the observed evolution of isotopic data in the entire water column with the multilayer model. The mean annual groundwater inflow determined from the well-mixed model was found to be 1.4 times lower than that determined from the multilayer model.

4.3.2 | The ^{222}Rn-based model

Similar to the water stable isotope model described above, a model of lake ^{222}Rn activity (C_L) with a daily time step was proposed, and groundwater inflow (I_G) was determined to achieve the closest match between the measured and modelled values of C_L. A mean groundwater inflow of 201 m^3/day was found for the steady-state, well-mixed model to fit the volume-weighted mean ^{222}Rn activity in the lake (Figure 8).

For the multilayer ^{222}Rn mass balance model, a daily time step was found to be too long for such explicit time discretization and led to divergence of the model. The model was therefore run with an hourly time step. As for the water stable isotope model, the ^{222}Rn activity calculated for the lake was equal to the mean volume-weighted value at the time of autumn mixing (October 15th). The results of the ^{222}Rn mass balance multilayer model are presented in Figure 10. The mean annual groundwater inflow obtained to fit the ^{222}Rn data is 161 m^3/day. Figure 10 also shows the groundwater fluxes obtained for the different layers. During summer, the groundwater inflow was higher in the deepest part of the lake (55 m^3/day) than in the three other layers (26 m^3/day for the 0- to 2-m layer and 13 m^3/day for the two middle ones). In mid-December, fluxes in the 2- to 3-m-deep layer increased to 96 m^3/day, and remained relatively low at the other depths. By the beginning of March, groundwater inflow decreased in the 2- to 3-m layer but increased in 0- to 2-m layer (from 26 to 233 m^3/day), as well as in the 4- to 5.5-m layer (from 26 to 130 m^3/day), probably

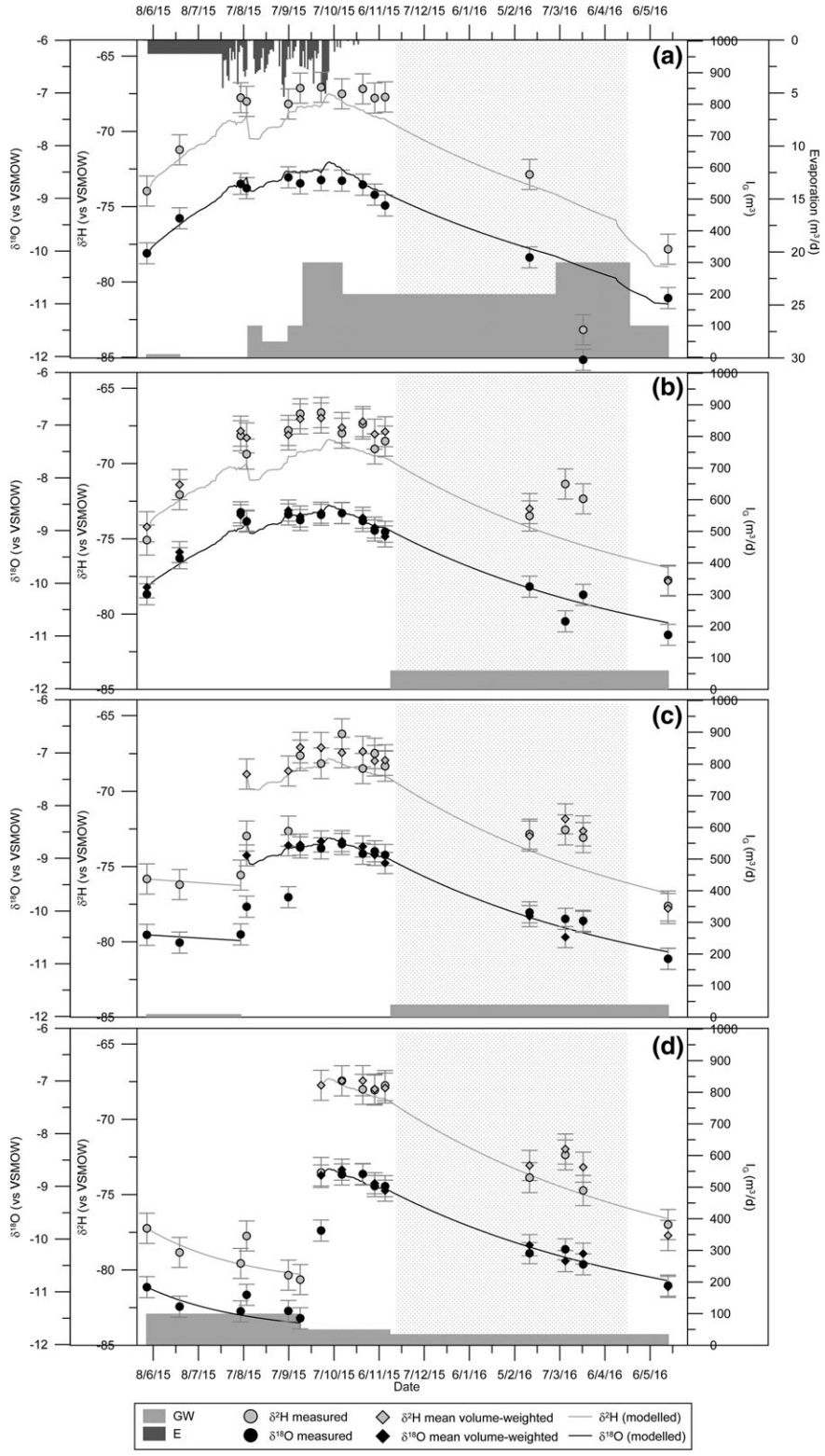

FIGURE 9 Measured and modelled lake water $\delta^{18}O$ and $\delta^{2}H$ evolutions at various depths (a. 0–2 m depth, b. 2–3 m, c. 3–4 m, and d. 4–5.5 m), and groundwater inflow at each depth, determined by the multilayer isotope mass balance model. The ice-covered period, from November 15th to May 10th, is represented by the grey area

due to snow melt in the catchment. Finally, at the end of April, groundwater inflow decreased to 52 and 78 m^3/day in the 0- to 2-m and 4- to 5.5-m layers, respectively.

4.3.3 | Sensitivity analyses

In order to investigate the uncertainty associated with the main model parameters, sensitivity analyses were conducted. For each parameter, two cases were considered, with values higher and lower than the value used, using a chosen standard deviation as the increment. Groundwater inflow was then calculated and compared with the reference case. Results are presented in Table 2 for the water stable isotope model and in Table 3 for the ^{222}Rn model.

As summarized in Table 2, the isotopic model is not particularly sensitive to uncertainties in lake volume, precipitation, or temperature but is highly sensitive to changes in δ_A, *h*, and *E* during the evaporation period (from June to October) and to changes in δ_G during the ice-covered period (from November to May). The ^{222}Rn mass balance model is

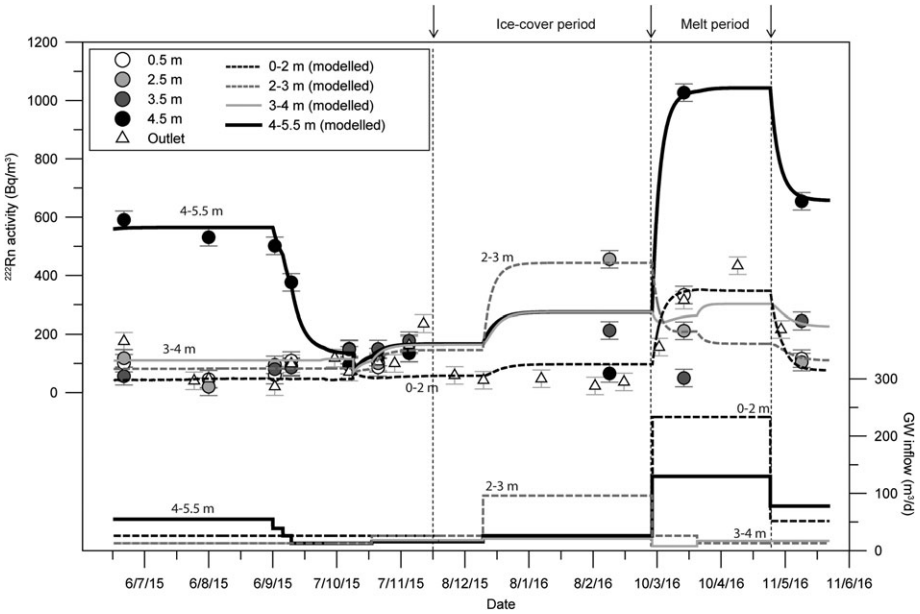

FIGURE 10 Measured and modelled lake water ^{222}Rn activity evolutions at various depths and in the outlet stream, and groundwater inflow calculated in the different layers from the ^{222}Rn mass balance model. The ice-covered period, from November 15th to May 10th, is represented by the grey area

TABLE 2 Sensitivity analysis for the water stable isotope mass balance model; τ is the mean lake flushing time by groundwater and *R* is the equivalent recharge on the lake catchment

Test	I_G in the 0-to 2-m layer (m^3/day)	I_G in the 2- to 3-m layer (m^3/day)	I_G in the 3- to 4-m layer (m^3/day)	I_G in the 4- to 5.5-m layer day	Mean annual I_G (m^3/day)	τ_{GW} (day) $\tau = V_L/I_G$	*R* (mm/year) $R = I_G/A_C$
Reference case	164	32	23	57	276	244	679
V_L ± 10%	No significant change						
$\delta_A{}^2H$ + 23.58‰ $\delta_A{}^{18}O$ + 2.70‰	309	37	24	48	418	161	1,028
$\delta_A{}^2H$ − 23.58‰ $\delta_A{}^{18}O$ − 2.70‰	Not possible to fit data						
E Penman with Dalton coefficient = 0.9	241	38	23	48	350	193	861
E Penman with Dalton coefficient = 0.2	138	32	23	48	241	280	593
$\delta_G{}^2H$ − 1.83‰ $\delta_G{}^{18}O$ − 0.32‰	144	28	20	42	234	288	576
$\delta_G{}^2H$ + 1.83‰ $\delta_G{}^{18}O$ + 0.32‰	183	42	29	109	363	186	893
h + 10%	Not possible to fit data						
h − 10%	196	38	24	57	315	214	775
T ± 10%	No significant change						
P ± 10%	No significant change						

highly sensitive to groundwater ^{222}Rn activity, which is known and was measured to be highly variable in both space and time. This therefore leads to a high range of uncertainty. Indeed, if a high groundwater ^{222}Rn activity is used in the model (e.g., 19,606 Bq/m^3), a mean annual groundwater inflow of 388 m^3/day is obtained; much higher than the value obtained in the reference case (Table 3). This value is indeed unrealistically high, because it suggests a 174-day flushing time of the lake by groundwater and an equivalent recharge equal to 954 mm/year, while recharge is estimated to be approximately 500 mm/year for sandy surfaces, as is partially the case Lake Lacasse area (Leblanc, Légaré, Lacasse, Parent, & Campeau, 2013). Conversely, low groundwater ^{222}Rn activity (e.g., 5,537 Bq/m^3) leads to a mean groundwater flushing time of 661 days, longer than that of the reference case (465 days). Groundwater inflow from the ^{222}Rn model is quite sensitive to uncertainty in the volumes assigned to the various layers, but not sensitive to uncertainty in the sediment fluxes, in the degassing coefficient (*k*) and in areas of layer interfaces.

5 | DISCUSSION

5.1 | Comparison of the tracers

This study shows that both water stable isotopes and ^{222}Rn are good tracers of groundwater inflow variation in a small lake. The ^{222}Rn has been found to be more horizontally variable than water stable isotopes,

TABLE 3 Sensitivity analysis for the ^{222}Rn mass balance model; τ is the mean lake flushing time by groundwater, and *R* is the equivalent recharge on the lake catchment

Test	I_G in the 0-to 2-m layer (m^3/day)	I_G in the 2- to 3-m layer (m^3/day)	I_G in the 3- to 4-m layer (m^3/day)	I_G in the 4- to 5.5-m layer day	Mean annual I_G (m^3/day)	τ_{GW} (day) $\tau = V_L/I_G$	*R* (mm/year) $R = I_G/A_C$
Reference case	60	34	16	51	161	419	396
Groundwater activity + 7,035 Bq/m^3	145	80	38	124	388	174	954
Groundwater activity − 7,035 Bq/m^3	39	21	10	32	102	661	251
Volume layers + 10%	60	37	16	55	168	401	414
Volume layers − 10%	51	33	14	46	144	467	355
k ± 10%	No significant change						
F_{sed} ± 0.2 Bq·m^{-2}·day^{-1}	No significant change						
Interface areas ± 10%	No significant change						

which follow a smoother evolution in both time and space. Both tracers follow the hydrological cycle of the lake during stratification in summer and during the autumn mixing period. Variations during winter and spring are quite different between the two tracers; ^{222}Rn is affected by winter stratification, whereas water stable isotopes present a homogenous water column for the same period. This ^{222}Rn winter stratification is attributed to substantial groundwater input to the lake as of the beginning of March, due to a short period of melt. Both tracers are sensitive to this increase in groundwater inflow, but ^{222}Rn appears to be more sensitive to its vertical location, which appears to mainly be concentrated at the surface and in the deepest part of the lake.

During winter and until the beginning of March, the isotopic model predicted relatively constant groundwater inflow, decreasing with depth, whereas the ^{222}Rn model suggested an increase in groundwater inflow in the 2 to 3–m-depth layer with constant and low groundwater inflow in the other three layers. The beginning of March was impacted by a 10-day mild spell, which had a substantial impact on local hydrogeology, increasing water levels in wells (Figure 3) and groundwater inflow to the lake. Both isotopic and ^{222}Rn models confirmed this, with increased groundwater input in the 0 to 2–m layer (233 and 300 m^3/day with the ^{222}Rn and isotopic models, respectively) from the beginning of March to the end of April. Finally, ^{222}Rn seems to be more sensitive than water stable isotopes to rapid changes in groundwater inflow. In the summer, both tracers show stronger groundwater input in the deep water (from 55 to 100 m^3/day) than near the surface (from 10 to 26 m^3/day). During autumn, groundwater inflow decreases in the deepest strata of the lake, as inferred by both models.

Total groundwater inflow to the lake was underestimated by the well-mixed water stable isotopic model, with a mean value of 198 m^3/day versus 276 m^3/day obtained from the multilayer model. Indeed, the well-mixed model was unable to accurately resolve groundwater inflow when evaporation occurred at the lake surface. Conversely, the well-mixed ^{222}Rn model overestimated the mean annual groundwater inflow to the lake, with a mean value of 201 m^3/day compared to 161 m^3/day obtained from the multilayer model.

5.2 | Lake hydrological balance and behaviour

The high-resolution depth monitoring carried out in the current work has revealed the locations of groundwater fluxes. In previous studies, groundwater fluxes have been described as being mainly localized in the shallow layer of the lake, the deep layer being less permeable because of fine sediment deposits (Hinton, 2014; Kluge et al., 2012). For Lake Lacasse, they appear mainly in the deepest layer in the summer. It is possible that groundwater inputs to the deeper layer of this lake may be supported by the presence of fractured bedrock, through which water flows during the summer. This suggests that it is the underlying geological formations, rather than lake bed sediments, that control the observed seepage patterns (Kidmose, Engesgaard, Nilsson, Laier, & Looms, 2011; Schneider, Negley, & Wafer, 2005). However, it is more likely that this seepage pattern is due to the difference in temperatures and therefore density, as already suggested by Kluge et al. (2012). Indeed, groundwater inflow, with a mean temperature of 7 °C, is denser than the lake water in the summer and can thus enter in the shallow layer and sink to the deeper layer. Our results agree with previous studies that have concluded that groundwater inflow to lakes can be highly variable in time and space (Kidmose et al., 2011; Schmidt et al., 2010).

Lake Lacasse appears to be highly and rapidly sensitive to changes in groundwater fluxes. Our interpretation of lake dynamics is that, in the summer, the water column warms, so that the groundwater that feeds the lake, which is denser, stagnates preferentially at the bottom of the lake, thus increasing the relative proportion of the groundwater inflows to the bottom layer. However, these contributions remain relatively low due to the decreased hydraulic gradient induced by the absence of (or very low) recharge. In autumn, as the thermal gradient decreases within the lake, the water column mixes and becomes homogeneous. At the same time, groundwater flows intensify due to increased recharge, as highlighted by the tracers throughout the water column. During the winter, under ice cover, the groundwater flows remain relatively constant, due to the low recharge at this time. During the melt period, (a) water resulting from snow melt in the watershed runs off into the lake under the ice cover (because it is approximately 0 °C and therefore less dense than the lake water), and (b) recharge increases, resulting in the rapid increase in piezometric levels and quasi-instantaneous intensification of groundwater inputs into the lake. The ^{222}Rn peak observed at the bottom of the lake can be explained by this groundwater loading and the small difference in density between the groundwater and the lake water at this time. Surface meltwater is then quickly evacuated through the outlet stream of the lake. In spring, after snow melt, recharge decreases sharply and groundwater flows decrease slowly, while continuing to feed the lake's water column, which mixes at approximately 4 °C.

According to the literature, mean annual recharge in fluvioglacial deposits is estimated to be between 300 and 500 mm/year (Leblanc et al., 2013), and the result obtained here is probably overestimated due to the uncertainty in δ_A and evaporation, neither measured directly in the field. A groundwater inflow of 276 m^3/day, estimated from the multilayer isotopic model, corresponds to a flushing time of 0.67 years and is equal to a recharge of 679 mm/year. The groundwater inflow of 161 m^3/day, estimated from the multilayer ^{222}Rn model, corresponds to a flushing time of 1.15 years and is equivalent to a recharge rate of 396 mm/year, which is reasonable considering the local hydroclimatic conditions. The difference between the two methods may reflect higher ^{222}Rn reactivity that was not fully captured with the biweekly to monthly sampling time interval.

2015–2016 is considered to be a representative year, even though it is slightly warm and wet. Data recorded at the Saint-Faustin-Lac-Carré station give an average precipitation and temperature from June 2015 to May 2016 of 1,213 mm and 5.7 °C, respectively, whereas annual averages for the area are estimated to be 1,100 mm and 3.5 °C, based on data from 1900 to 2010, reviewed by the Québec Center of Expertise (Poirier, Fortier Filion, Turcotte, & Lacombe, 2014). Lacasse Lake is dominated by groundwater, which accounts for an average of 72% of total lake inflows based on the multilayered isotopic model and 59% based on the ^{222}Rn model. The mean annual flow measured at the outlet is approximately 112,400 m^3/year. Given that the isotopic model is closer to reality than the radon model, because of smaller uncertainties (see the results of the sensitivity analysis), total lake outflows would be mainly through the surface outlet of the lake and, based on the multilayered isotopic model, only about 3,800 m^3/year would infiltrate into groundwater. Therefore, it appears that outlet gauging for this type of lake could provide a reasonable estimate of the total inflows. Moreover, it can be noted that if only one sampling campaign is to be carried out to characterize groundwater inflows to a lake, results of this study suggest that sampling at the time of autumn mixing would be best to avoid water column stratification.

5.3 | Methodological limitations

A steady state was assumed in the models while lake level slightly varies during the year (Figure 3). However, violations of this assumption are likely to have a small effect on the results, given $I_G >> dV/dt$.

The ^{222}Rn multilayer model allowed the characterization of vertical heterogeneity in groundwater inflow. However, when only limited data are available throughout a given year, its higher reactivity makes it more difficult to determine annual or seasonal water budgets. In contrast, the stable isotopic approach seems well adapted for longer term assessments of changes in groundwater inflow. The methods are each sensitive to different factors; the ^{222}Rn method requires good knowledge of groundwater activity, which is very difficult to achieve due to high ^{222}Rn activity heterogeneity in groundwater and therefore benefits from sampling several wells around the lake. The water stable isotope–based approach is sensitive to local humidity, evaporation, and δ_A input. The two tracers are clearly complementary, and their combined application improves our understanding and confidence in the overall results. In addition, ^{222}Rn equilibrium assumption can be influenced by storm events (Gilfedder et al., 2015). Sampling did not occur just after heavy rain or high wind events; therefore, we assumed that this would not significantly influence our results, especially the yearly ones. However, further work with shorter sampling step could be interesting to determine how ^{222}Rn activity, sensitive to short variations in groundwater inflows, varies on shorter time scale in this kind of lake, to improve the accuracy of our model.

This paper proposes simple calculations to better understand the dynamics of groundwater inflows to a lake. The use of two different types of tracers allows us to discuss their relevance to quantifying groundwater fluxes. However, the complete lake dynamics are not taken into account; short periods of incomplete advection, if occur, are not modelled in this study, which considers only two periods of full mixing in the spring and autumn and adapts the number of layers and exchange between them throughout the year. Moreover, ice cover is considered to go from 0% to 100% instantaneously by mid-November and similarly from 100% to 0% during the melt period. The rest of the time, the lake area is assumed to be constant. This assumption does not significantly change our results, but it is nonetheless a simplification of real lake dynamics.

6 | CONCLUSIONS

In this study, the dynamics of the natural tracers, ^{222}Rn and $^{18}O/^{2}H$, were determined for a small, groundwater-connected lake. It has been shown that both water stable isotopes and ^{222}Rn are good tracers to infer variations of the internal dynamics of the lake and groundwater inflow. These tracers follow lake dynamics through summer stratification and homogenisation of the water column in autumn. During winter and spring, the two tracers diverge, showing a well-mixed water column, with a homogeneous stable water isotopic composition, and a stratified water column with ^{222}Rn. Moreover, both tracers reflect the variable groundwater inflow to the lake. They both show (a) low groundwater input during the summer, with stronger input in the deepest part of the lake; (b) decreasing input to the deepest part and increasing input to the surface during autumn; followed by (c) medium input during the winter, mostly to the surface; and, finally, (d) substantial groundwater input to the lake during the melt period. Moreover, the ^{222}Rn model highlights substantial and fast groundwater input as of the beginning of March, due to a short period of melt. Indeed, ^{222}Rn appears to be more sensitive than water stable isotopes to rapid changes in groundwater inflow, whereas the stable isotopic approach seems well-adapted to longer term assessments of changes in groundwater inflow. The ^{222}Rn method requires good knowledge of groundwater dynamics, while the water stable isotope–based approach is very sensitive to local meteorological parameters. The two tracers have been shown to be complementary, and combining them is suggested to improve our understanding of groundwater–lake interactions.

As much as possible, tracer evolution should be determined with depth throughout the entire water column; a depth-resolved multilayer model is a better approach than a well-mixed model in using ^{222}Rn and water stable isotopes mass balances to determine groundwater–lake interactions, allowing the vertical location of the groundwater inflows.

Even though a well-mixed volume-weighted model could also be used and would lead to similar results, the evolution of the tracers throughout the entire water column has been shown to be important to measure, and not only at the outlet, which only represents the composition of the lake's surface. Finally, this study shows that the precise monitoring of lake geochemical composition highlights changes in groundwater fluxes in time and helps to better understand lake dynamics.

REFERENCES

Ala-aho, P., Rossi, P. M., Isokangas, E., & Kløve, B. (2015). Fully integrated surface–subsurface flow modelling of groundwater–lake interaction in an esker aquifer: Model verification with stable isotopes and airborne thermal imaging. *Journal of Hydrology*, *522*, 391–406. https://doi.org/10.1016/j.jhydrol.2014.12.054

Alazard, M., Leduc, C., Travi, Y., Boulet, G., & Ben, S. A. (2015). Estimating evaporation in semi-arid areas facing data scarcity: Example of the El Haouareb dam (Merguellil catchment, Central Tunisia). *Journal of Hydrology: Regional Studies*, *3*, 265–284. https://doi.org/10.1016/j.ejrh.2014.11.007

Arnoux, M., Barbecot, F., Gibert-Brunet, E., Gibson, J., Rosa, E., Noret, A., & Monvoisin, G. (2017). Geochemical and isotopic mass balances of kettle lakes in southern Quebec (Canada) as tools to document variations in groundwater quantity and quality. *Environmental Earth Sciences*, *76*(3), 106. https://doi.org/10.1007/s12665-017-6410-6

Baudron, P., Cockenpot, S., Lopez-Castejon, F., Radakovitch, O., Gilabert, J., Mayer, A., … Claude, C. (2015). Combining radon, short-lived radium isotopes and hydrodynamic modeling to assess submarine groundwater discharge from an anthropized semiarid watershed to a Mediterranean lagoon (Mar Menor, SE Spain). *Journal of Hydrology*, *525*, 55–71. https://doi.org/10.1016/j.jhydrol.2015.03.015

Cable, J. E., Burnett, W. C., Chanton, J. P., & Weatherly, G. L. (1996). Estimating groundwater discharge into the northeastern Gulf of Mexico using radon-222. *Earth and Planetary Science Letters*, *144*, 591–604

Cook, P. G., Wood, C., White, T., Simmons, C. T., Fass, T., & Brunner, P. (2008). Groundwater inflow to a shallow, poorly-mixed wetland estimated from a mass balance of radon. *Journal of Hydrology*, *354*, 213–226. https://doi.org/10.1016/j.jhydrol.2008.03.016

Corbett, D. R., Burnett, W. C., Cable, P. H., & Clark, S. B. (1997). Radon tracing of groundwater input into Par Pond, Savannah River site. *Journal of Hydrology*, *203*, 209–227. https://doi.org/10.1016/S0022-1694(97)00103-0

Corbett, D. R., Burnett, W. C., Cable, P. H., & Clark, S. B. (1998). A multiple approach to the determination of radon fluxes from sediments. *Journal of Radioanalytical and Nuclear Chemistry*, *236*, 247–252. https://doi.org/10.1007/BF02386351

Craig, H., & Gordon, L. I. (1965). Deuterium and oxygen-18 in the ocean and marine atmosphere. In E. Tongiorgi (Ed.), *Stable isotopes in oceanographic studies and Paleotemperatures* (pp. 9–130). Spoleto, Italy

von Rohden, C., Ilmberger, J., & Boehrer, B. (2009). Assessing groundwater coupling and vertical exchange in a meromictic mining lake with an SF6-tracer experiment. *Journal of Hydrology*, *372*, 102–108. https://doi.org/10.1016/j.jhydrol.2009.04.004

Dinçer, T., & Davis, G. H. (1984). Application of environmental isotope tracers to modeling in hydrology. *Journal of Hydrology*, *68*, 95–113. https://doi.org/10.1016/0022-1694(84)90206-3

Gibson, J. J. (2002). Short-term evaporation and water budget comparisons in shallow Arctic lakes using non-steady isotope mass balance. *Journal of Hydrology*, *264*, 242–261. https://doi.org/10.1016/S0022-1694(02)00091-4

Gibson, J. J., Birks, S. J., & Yi, Y. (2015). Stable isotope mass balance of lakes: A contemporary perspective. *Quaternary Science Reviews*, *131*, 316–328. https://doi.org/10.1016/j.quascirev.2015.04.013

Gilfedder, B. S., Frei, S., Hofmann, H., & Cartwright, I. (2015). Groundwater discharge to wetlands driven by storm and flood events: Quantification using continuous radon-222 and electrical conductivity measurements and dynamic mass-balance modelling. *Geochimica et Cosmochimica Acta*, *165*, 161–177. https://doi.org/10.1016/j.gca.2015.05.037

Gleeson, T., Novakowski, K., Cook, P. G., & Kyser, T. K. (2009). Constraining groundwater discharge in a large watershed: Integrated isotopic, hydraulic, and thermal data from the Canadian shield. *Water Resources Research*, *45*, n/a–n/a. https://doi.org/10.1029/2008wr007622

Gonfiantini, R. (1986). Environmental isotopes in lake studies. In P. Fritz, & J. C. Fontes (Eds.), *Handbook of environmental isotope geochemistry* (Vol. 3) (pp. 113–168)

Gröning, M., Lutz, H. O., Roller-Lutz, Z., Kralik, M., Gourcy, L., & Pöltenstein, L. (2012). A simple rain collector preventing water re-evaporation dedicated for δ18O and δ2H analysis of cumulative precipitation samples. *Journal of Hydrology*, *448-449*, 195–200. https://doi.org/10.1016/j.jhydrol.2012.04.041

Hinton, M. J. (2014). Groundwater-surface water interactions in Canada. In A. Rivera (Ed.), *Canada's groundwater resources* (pp. 151–185). Canada

Horita, J., Rozanski, K., & Cohen, S. (2008). Isotope effects in the evaporation of water: A status report of the Craig-Gordon model. *Isotopes in Environmental and Health Studies*, *44*, 23–49. https://doi.org/10.1080/10256010801887174

Horita, J., & Wesolowski, D. (1994). Liquid-vapour fractionation of oxygen and hydrogen isotopes of water from the freezing to the critical temperature. *Geochimica et Cosmochimica Acta*, *58*, 3425–3437

Hunt, R. J., Haitjema, H. M., Krohelski, J. T., & Feinstein, D. T. (2003). Simulating ground water-lake interactions: Approaches and insights. *Ground Water*, *41*, 227–237. https://doi.org/10.1111/j.1745-6584.2003.tb02586.x

Imboden, D. M., & Joller, T. (1984). Turbulent mixing in the hypolimnion of Baldeggersee (Switzerland) traced by natural radon-222. *Limnology and Oceanography*, *29*, 831–844

Isokangas, E., Rozanski, K., Rossi, P. M., Ronkanen, A. K., & Kløve, B. (2015). Quantifying groundwater dependence of a sub-polar lake cluster in Finland using an isotope mass balance approach. *Hydrology and Earth System Sciences*, *19*, 1247–1262. https://doi.org/10.5194/hess-19-1247-2015

Kidmose, J., Engesgaard, P., Nilsson, B., Laier, T., & Looms, M. C. (2011). Spatial distribution of seepage at a flow-through lake: Lake Hampen, western Denmark. *Vadose Zone Journal*, *10*, 110–124. https://doi.org/10.2136/vzj2010.0017

Kidmose, J., Nilsson, B., Engesgaard, P., Frandsen, M., Karan, S., Landkildehus, F., … Jeppesen, E. (2013). Focused groundwater discharge of phosphorus to a eutrophic seepage lake (Lake Væng, Denmark): Implications for lake ecological state and restoration. *Hydrogeology Journal*, *21*, 1787–1802. https://doi.org/10.1007/s10040-013-1043-7

Kiro, Y., Yechieli, Y., Voss, C. I., Starinsky, A., & Weinstein, Y. (2012). Modeling radium distribution in coastal aquifers during sea level changes: The Dead Sea case. *Geochimica et Cosmochimica Acta*, *88*, 237–254. https://doi.org/10.1016/j.gca.2012.03.022

Kluge, T., Ilmberger, J., von Rohden, C., & Aeschbach-Hertig, W. (2007). Tracing and quantifying groundwater inflow into lakes using a simple method for radon-222 analysis. *Hydrology and Earth System Sciences*, *11*, 1621–1631

Kluge, T., von Rohden, C., Sonntag, P., Lorenz, S., Wieser, M., Aeschbach-Hertig, W., & Ilmberger, J. (2012). Localising and quantifying groundwater inflow into lakes using high-precision 222Rn profiles. *Journal of Hydrology*, *450-451*, 70–81. https://doi.org/10.1016/j.jhydrol.2012.05.026

Krabbenhoft, D. P., Bowser, C. J., Anderson, M. P., & Valley, J. W. (1990). Estimating groundwater exchange with lakes. 1. The stable isotope mass balance method. *Water Resources Research*, *26*, 2445–2453. https://doi.org/10.1029/90wr01135

Leblanc, Y., Légaré, G., Lacasse, K., Parent, M., & Campeau, S. (2013). Caractérisation hydrogéologique du sud-ouest de la Mauricie. Rapport déposé au ministère du Développement durable, de l'Environnement,

de la Faune et des Parcs dans le cadre du Programme d'acquisition de connaissances sur les eaux souterraines du Québec. Département des sciences de l'environnement, Université du Québec à Trois-Rivières, 134 p., 15 annexes et 30 documents cartographiques (1:100000)

Lefebvre, K., Barbecot, F., Ghaleb, B., Larocque, M., & Gagne, S. (2013). Full range determination of ^{222}Rn at the watershed scale by liquid scintillation counting. *Applied radiation and isotopes: including data, instrumentation and methods for use in agriculture, industry and medicine*, *75*, 71–76. https://doi.org/10.1016/j.apradiso.2013.01.027

Lewandowski, J., Meinikmann, K., Nützmann, G., & Rosenberry, D. O. (2015). Groundwater—the disregarded component in lake water and nutrient budgets. Part 2: Effects of groundwater on nutrients. *Hydrological Processes*, *29*, 2922–2955. https://doi.org/10.1002/hyp.10384

MacIntyre, S., Wanninkhof, R., & Chanton, J. P. (1995). Trace gas exchange across the air–water interface in freshwater and coastal marine environments. In P. A. Matson, & R. C. Harris (Eds.), *Biogenic trace gases: Measuring emissions from soil and water* (pp. 52–97). Massachusetts: Blackwell, Cambridge

Malgrange, J., & Gleeson, T. (2014). Shallow, old, and hydrologically insignificant fault zones in the Appalachian orogen. *Journal of Geophysical Research: Solid Earth*, *119*, 346–359. https://doi.org/10.1002/2013jb010351

MDDELCC (2016). Ministère du Développement durable, de l'Environnement et de la Lutte contre les changements climatiques; http://wwwmddelccgouvqcca

Poirier, C., Fortier Filion, T-C., Turcotte, R., & Lacombe, P. (2014). Reconstitution historique des apports verticaux (eaux de fonte et de pluie) de 1900 à 2010—version 2012 contribution au Programme d'Acquisition de Connaissances sur les Eaux Souterraines (PACES) Centre d'expertise hydrique du Québec (CEHQ), Direction de l'expertise hydrique, Québec, 99 p

Sacks, L. A., Lee, T. M., & Swancar, A. (2014). The suitability of a simplified isotope-balance approach to quantify transient groundwater–lake interactions over a decade with climatic extremes. *Journal of Hydrology*, *519*, 3042–3053. https://doi.org/10.1016/j.jhydrol.2013.12.012

Schilling, K. E., Streeter, M. T., Quade, D., & Skopec, M. (2016). Groundwater loading of nitrate-nitrogen and phosphorus from watershed source areas to an Iowa Great Lake. *Journal of Great Lakes Research*, *42*, 588–598. https://doi.org/10.1016/j.jglr.2016.03.015

Schmidt, A., Gibson, J. J., Santos, I. R., Schubert, M., Tattrie, K., & Weiss, H. (2010). The contribution of groundwater discharge to the overall water budget of two typical Boreal lakes in Alberta/Canada estimated from a radon mass balance. *Hydrology and Earth System Sciences*, *14*, 79–89

Schmidt, A., & Schubert, M. (2007). Using radon-222 for tracing groundwater discharge into an open-pit lignite mining lake—A case study. *Isotopes in Environmental and Health Studies*, *43*, 387–400. https://doi.org/10.1080/10256010701705419

Schneider, R. L., Negley, T. L., & Wafer, C. (2005). Factors influencing groundwater seepage in a large, mesotrophic lake in New York. *Journal of Hydrology*, *310*, 1–16. https://doi.org/10.1016/j.jhydrol.2004.09.020

Shaw, G. D., White, E. S., & Gammons, C. H. (2013). Characterizing groundwater–lake interactions and its impact on lake water quality. *Journal of Hydrology*, *492*, 69–78. https://doi.org/10.1016/j.jhydrol.2013.04.018

Smerdon, B. D., Allen, D. M., Grasby, S. E., & Berg, M. A. (2009). An approach for predicting groundwater recharge in mountainous watersheds. *Journal of Hydrology*, *365*, 156–172. https://doi.org/10.1016/j.jhydrol.2008.11.023

Stets, E. G., Winter, T. C., Rosenberry, D. O., & Striegl, R. G. (2010). Quantification of surface water and groundwater flows to open- and closed-basin lakes in a headwaters watershed using a descriptive oxygen stable isotope model. *Water Resources Research*, *46*, n/a–n/a. https://doi.org/10.1029/2009wr007793

Turner, J. V., Allison, G. B., & Holmes, J. W. (1984). The water balance of a small lake using stable isotopes and tritium. *Journal of Hydrology*, *70*, 199–220. https://doi.org/10.1016/0022-1694(84)90122-7

Turner, S. M., Malin, G., Nightingale, P. D., & Liss, P. S. (1996). Seasonal variation of dimethyl sulphide in the North Sea and an assessment of fluxes to the atmosphere. *Marine Chemistry*, *54*, 245–262

Wanninkhof, R. (1992). Relationship between wind speed and gas exchange over the ocean. *Journal of Geophysical Research*, *97*, 7373–7382

Zhu, C., & Schwartz, F. W. (2011). Hydrogeochemical processes and controls on water quality and water management. *Elements*, *7*, 169–174. https://doi.org/10.2113/gselements.7.3.169

How to cite this article: Arnoux M, Gibert-Brunet E, Barbecot F, Guillon S, Gibson J, Noret A. Interactions between groundwater and seasonally ice-covered lakes: Using water stable isotopes and radon-222 multilayer mass balance models. *Hydrological Processes*. 2017;31:2566–2581. https://doi.org/10.1002/hyp.11206